Modeling the seasonal and interannual variability of the northern Gulf of California salinity

Luis Zamudio,[1] E. Joseph Metzger,[2] and Patrick Hogan[2]

[1] The 7 years (2003–2009) of output from a regional version of the Hybrid Coordinate Ocean Model (HYCOM) nested in global HYCOM are used to study the seasonal and interannual variability of the salinity in the northern Gulf of California (NGOC). Previous studies illustrate that the NGOC is characterized by an annual evaporation of ~0.9 m/yr. This evaporation generates high-sea-surface-salinity (SSS) water, which reaches a maxima in the NGOC (>37) and decreases to ~35 toward the entrance of the Gulf of California. The NGOC surface water is interannually modulated by fluctuations in evaporation and by fluctuations in the low-salinity water transported into the region by poleward eastern boundary currents. The fluctuations in the transport of low-salinity water are linked to the arrival of equatorially originated coastally trapped waves. The crucial role of the transport of low-salinity water for the interannual variability of SSS is illustrated by the 2006 and 2008 fall seasons, which include the lowest simulated salinity of the period 2003–2009. The lowest salinity in 2006 and 2008 cannot be explained solely by evaporation because 2006 was characterized by the largest evaporation of the period 2003–2009. However, the presence of the lowest-salinity environment can be attributed to the evaporation in conjunction with the largest upper ocean transport of low-salinity water carried to the NGOC by the 2006 and 2008 coastally trapped waves intensified poleward eastern boundary currents.

1. Introduction

[2] The northern Gulf of California (NGOC) is a shallow and semienclosed basin characterized by high-evaporation (0.9–0.95 m/yr) and high-sea-surface-salinity (SSS) waters (>37.0) [*Bray*, 1988; *Lavín and Organista*, 1988; *Lavín et al.*, 1998]. The high solar insolation, geographical isolation of the NGOC (which is surrounded by deserts and mountains) and the arrival of several cold fronts that transport cold, dry desert air into the region, all combine to produce high evaporation [*Bray*, 1988; *Lavín and Organista*, 1988; *Badan-Dangon et al.*, 1991; *Reyes and Lavín*, 1997; *López*, 1997].

[3] Based on hydrographic observations, *Alvarez-Borrego and Schwartzlose* [1979], *Bray* [1988], and *Lavín et al.* [1995, 1998] hypothesized that the high evaporation in the NGOC would produce high-SSS water. In particular, the data reported by *Lavín et al.* [1998] shows the highest salinity in the shallow upper NGOC. In the same line of research, *López* [1997] used a numerical ocean model to study the NGOC winter circulation and finds that as a result of cooling and evaporation, water in the shallow NGOC increases its density. Emphasizing the importance of the oceanic remote forcing, *Ripa* [1997] reported that most of the dynamics and thermodynamics of the Gulf of California (GOC) are controlled by the Pacific Ocean, which excites a baroclinic Kelvin wave at the entrance of the GOC. Based on the *Ripa's* [1997] Kelvin wave scenario, *Berón-Vera and Ripa* [2002] used a linear one-dimensional nondiffusive inhomogeneous two-layer model to study the salt balance in the GOC and found that the seasonal balance of the salinity is largely controlled by the Pacific Ocean.

[4] In addition to the several questions answered by these studies, some valid questions have not yet been answered. Is the NGOC high evaporation the essential generator and modulator of the NGOC high-salinity water? What is the role of the Costa Rica Coastal Current (CRCC) and the Mexican Coastal Current (MCC) on the seasonal evolution of the NGOC upper ocean water and upper ocean circulation? What is the role of equatorially forced coastally trapped waves (CTWs) on the interannual variability of the NGOC surface water?

[5] This work builds on the previous studies by documenting the NGOC seasonal evolution of SSS water, which has a strong interannual variability, and is modulated by the NGOC high evaporation, and by the CRCC and the MCC. To explain the origin of the seasonal and interannual salinity variability of the NGOC surface water, two hypotheses are presented and discussed. The first hypothesis is that evaporation is the primary generator and modulator. The second hypothesis builds on *Ripa's* [1997] model of the Pacific

---

[1]Center for Ocean-Atmospheric Prediction Studies, Florida State University, Tallahassee, Florida, USA.
[2]Naval Research Laboratory, Stennis Space Center, Mississippi, USA.

		Report Documentation Page		*Form Approved* *OMB No. 0704-0188*

Public reporting burden for the collection of information is estimated to average 1 hour per response, including the time for reviewing instructions, searching existing data sources, gathering and maintaining the data needed, and completing and reviewing the collection of information. Send comments regarding this burden estimate or any other aspect of this collection of information, including suggestions for reducing this burden, to Washington Headquarters Services, Directorate for Information Operations and Reports, 1215 Jefferson Davis Highway, Suite 1204, Arlington VA 22202-4302. Respondents should be aware that notwithstanding any other provision of law, no person shall be subject to a penalty for failing to comply with a collection of information if it does not display a currently valid OMB control number.

1. REPORT DATE **NOV 2010**	2. REPORT TYPE		3. DATES COVERED **00-00-2010 to 00-00-2010**
4. TITLE AND SUBTITLE **Modeling the seasonal and interannual variability of the northern Gulf of California salinity**			5a. CONTRACT NUMBER
			5b. GRANT NUMBER
			5c. PROGRAM ELEMENT NUMBER
6. AUTHOR(S)			5d. PROJECT NUMBER
			5e. TASK NUMBER
			5f. WORK UNIT NUMBER
7. PERFORMING ORGANIZATION NAME(S) AND ADDRESS(ES) **Naval Research Laboratory,Stennis Space Center,MS,39529**			8. PERFORMING ORGANIZATION REPORT NUMBER
9. SPONSORING/MONITORING AGENCY NAME(S) AND ADDRESS(ES)			10. SPONSOR/MONITOR'S ACRONYM(S)
			11. SPONSOR/MONITOR'S REPORT NUMBER(S)

12. DISTRIBUTION/AVAILABILITY STATEMENT
Approved for public release; distribution unlimited

13. SUPPLEMENTARY NOTES

14. ABSTRACT

15. SUBJECT TERMS

16. SECURITY CLASSIFICATION OF:			17. LIMITATION OF ABSTRACT **Same as Report (SAR)**	18. NUMBER OF PAGES **12**	19a. NAME OF RESPONSIBLE PERSON
a. REPORT **unclassified**	b. ABSTRACT **unclassified**	c. THIS PAGE **unclassified**			

Standard Form 298 (Rev. 8-98)
Prescribed by ANSI Std Z39-18

Table 1. Summary of the Main Features of the Simulations Used in This Study[a]

Experiment	Domain	Boundary Conditions From Experiment	Horizontal Resolution	Period (years)	Winds	Wind Frequency	Remote Forcing	CRCC	MCC	Annual CTW	Interannual CTW
1	Global	N/A	1/25°	1–10	ERA40/QuikSCAT	Monthly	N/A	Yes	Yes	Yes	No
2	Global	N/A	1/25°	2003–2009	NOGAPS/QuikSCAT	6 h	N/A	Yes	Yes	Yes	Yes
3	Nested GOC	1	1/25°	1–10	ERA40/QuikSCAT	Monthly	Yes	Yes	Yes	Yes	No
4	Nested GOC	1	1/25°	1–10	No Wind	Monthly	Yes	Yes	No	Yes	No
5	Nested GOC	N/A	1/25°	1–10	ERA40/QuikSCAT	Monthly	No	No	Yes	No	No
6	Nested GOC	2	1/25°	2003–2009	NOGAPS/QuikSCAT	6 h	Yes	Yes	Yes	Yes	Yes
7	Nested GOC	2	1/25°	2003–2009	No Wind	6 h	Yes	Yes	No	Yes	Yes
8	Nested GOC	N/A	1/25°	2003–2009	NOGAPS/QuikSCAT	6 h	No	No	Yes	No	No

[a]All the experiments included in this study contain 32 layers.

Ocean as the main forcing of the GOC. Thus, together these two hypotheses suggest that the evaporation in conjunction with the low-salinity water (~35) transported by the CRCC, the MCC, and the CTWs are responsible for the seasonal and interannual variability of the SSS. Our approach is based on the analysis of the results of three climatological and three interannual forced regional GOC Hybrid Coordinate Ocean Model (HYCOM) simulations, which are nested in global HYCOM. The nested approach allows the isolation of the effects of both local and remote forcings and the time period of the interannual simulations (2003–2009) allows the evaluation of the effects of the El Niño-La Niña cycle on the NGOC.

2. The Model

[6] The Hybrid Coordinate Ocean Model is isopycnal in the open stratified ocean, terrain following in shallow coastal regions, and maintains z levels in the mixed layer and unstratified regions. This generalized vertical coordinate approach is dynamic in space and time via the layered continuity equation that allows a smooth dynamical transition between the coordinate types. HYCOM [*Bleck*, 2002] was developed from the Miami Isopycnic Coordinate Ocean Model using the theoretical foundation for implementing a hybrid coordinate system [*Bleck and Benjamin*, 1993]. Application of HYCOM to the GOC has been discussed by *López et al.* [2005] and *Zamudio et al.* [2008, 2010].

[7] Two different eddy-resolving (1/25° equatorial resolution) HYCOM configurations are used. The global model (which is the provider of boundary conditions for the nested GOC model) is on a Mercator projection from 78.64°S to 47°N and north of this it employs an Arctic dipole patch where the poles are shifted over land to avoid a singularity at the North Pole. The nested GOC model is on a Mercator projection and extends from 118°W to 97°W and 14°N to 32°N. The global model was initialized using temperature and salinity from the Generalized Digital Environmental Model (GDEM) Version 3.0 climatology [*Carnes*, 2009]. Next, it was spun-up for 10 years using a monthly climatology based on the 1979–2002 1.125° European Centre for Medium-Range Weather Forecasts (ECMWF) 40 year reanalysis (ERA40) [*Kallberg et al.*, 2004] using the bulk formulation of *Kara et al.* [2005a] for converting 10 m winds to wind stress and with the wind speeds corrected using a regression to a monthly climatology from QuikSCAT scatterometer data [*Kara et al.*, 2009], i.e., ERA40-QuikSCAT, as previously implemented by *Metzger et al.* [2010]. In addition, the model is driven by daily averaged surface air

temperature, surface atmospheric humidity, surface short-wave and long-wave heat fluxes, and precipitation. Surface latent and sensible heat fluxes and evaporation are calculated at each model time step using the model's top layer temperature [*Kara et al.*, 2005a]. Furthermore, the model includes monthly rivers [*Barron and Smedstad*, 2002] and turbidity forcing [*Kara et al.*, 2005b], realistic bottom topography and coastline geometry, which are based on a modified version of the NRL DBDB2 topography (http://www7320.nrlssc.navy.mil/DBDB2_WWW). The model uses the 5 m isobath as a land-sea boundary, includes 32 vertical coordinate layers, allows isopycnals to intersect sloping topography by allowing zero thickness layers, does not include ocean data assimilation, and relaxes the sea surface salinity toward the Polar Science Center Hydrographic Climatology [*Steele et al.*, 2001]. This is required to prevent long-term SSS drift due to inadequate precipitation minus evaporation forcing. After spin-up, the model used the Fleet Numerical Meteorology and Oceanography Center (FNMOC) 3 hourly 0.5° Navy Operational Global Atmospheric Prediction System (NOGAPS) forcing [*Rosmond et al.*, 2002] spanning the time frame 2003–2009. For the wind forcing, the long-term (annual) mean from NOGAPS was replaced by ERA40 mean for consistency on the larger scale as discussed by *Metzger et al.* [2010].

[8] The nested GOC HYCOM was similarly initialized and forced as the global model in both climatological and interannual modes. However, lateral boundary conditions for the nested model were provided by global HYCOM. In addition, because the Colorado river in the NGOC region has been dammed [e.g., *Carbajal et al.*, 1997; *Lavín and Sánchez*, 1999], the nested model does not include any river input and the SSS is not relaxed to any climatology. The comparison of model results and observations of section 3.1 validates this approach. All the simulations discussed in the present study are included in Table 1. Furthermore, section 3.2.1 describes the application of the different nested simulations to separate the circulation induced by local and remote forcings.

3. Results and Discussion

3.1. Annual Salinity

[9] The long-term mean SSS of the GOC is characterized by a minimum of ~35 at the entrance of the GOC (Figure 1a). That increases toward the NGOC and reaches the maximum of ~36.6 at the upper GOC and incorporates the inverse estuarine features of the upper NGOC (maximum salinity at the head of the NGOC), which were previously documented
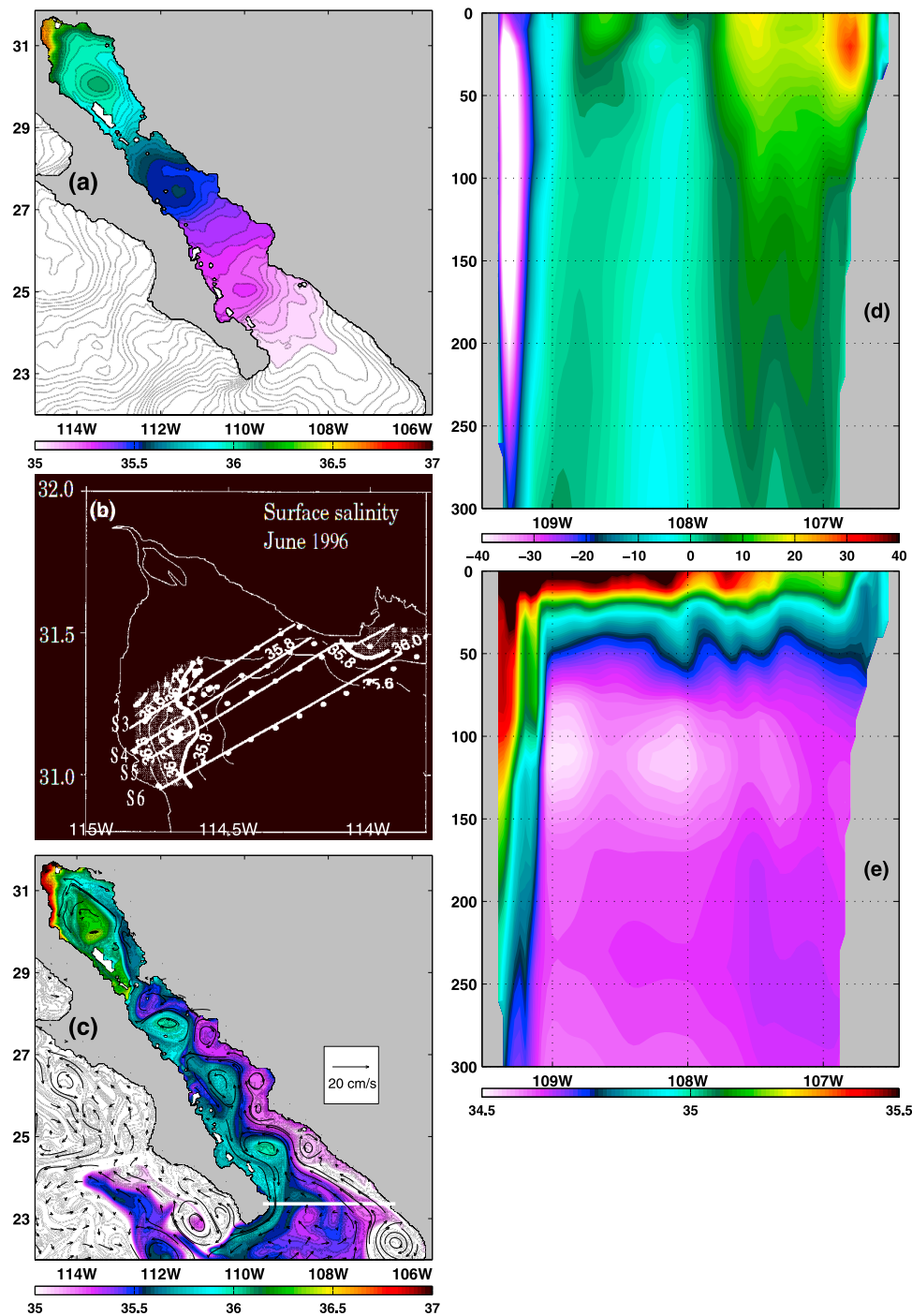
Figure 1. (a) The 5 year mean sea surface salinity (color contours) as determined by a climatologically forced nested GOC HYCOM simulation (experiment 3 in Table 1). (b) Sea surface salinity for 23 June to 1 July 1996. Adapted from *Lavín et al.* [1998], with permission from Elsevier. (c) Sea surface salinity (color contours) and upper ocean (0–100 m) currents (arrow vectors) for 23 June 2006 as determined by an interannually forced nested GOC HYCOM simulation (experiment 6 in Table 1). The upper ocean transport of Figure 6c was calculated along the white zonal line located at the entrance of the GOC. (d) Meridional currents (color contours in cm/s) and (e) salinity for 23 June 2006 along the white zonal line at the entrance of the GOC in Figure 1c.

by *Lavín et al.* [1998] (Figure 1b). Although the model simulates the observed inverse estuarine features of the upper NGOC, the comparison of the SSS of Figures 1a and 1b might suggest that the model underestimates the magnitude of the

maximum observed SSS of ~37.0. However, it is important to keep in mind that Figure 1a depicts a 5 year mean of simulated SSS whereas Figure 1b depicts the instantaneous observed SSS during a few days in early summer of 1996. So, to pro-

vide some insight on the validation of the model results, Figure 1c shows a simulated instantaneous SSS field during early summer of 2008 that features a maximum SSS of ~37.1 and this compares better with the maximum observed SSS of ~37.0. Even though the simulations of Figure 1 do not include tides, and consequently they do not include tidal mixing (which has been proposed as an important mechanism affecting the distribution of the salinity in the NGOC [e.g., *Argote et al.*, 1995; *Lavín et al.*, 1998]), they simulate the general characteristics of the GOC SSS reported in the literature.

[10] The instantaneous SSS field displays low-salinity water transported to the north by the poleward eastern boundary currents (PEBC) along the west coast of mainland Mexico (Figure 1c). During this day the PEBC extend from the surface to ~50 m depth and advect water with salinity values <35 (Figures 1d and 1e). The low-salinity tongue extends from the entrance of the GOC (with salinity <35) to the NGOC (with salinity of >37.0) and during its northward advection is modified (increasing its salinity) by the water of the GOC. In addition to a strong latitudinal gradient (which increases northward, reaches the maximum in the NGOC, and it is included in both the instantaneous and the long-term field), the instantaneous SSS field is characterized by a longitudinal gradient that increases westward and reaches the maximum along the eastern coast of the Baja California Peninsula (Figure 1c) as measured by *Lavín et al.* [1998] and *Castro et al.* [2000]. This salinity maximum is not limited to the sea surface, it extends to ~125 m depth and it is advected southward by a narrow western boundary equatoward current (Figures 1d and 1e).

3.2. Monthly Salinity and Circulation

3.2.1. Separation of Circulation Induced by Local and Remote Forcings

[11] Considering that monthly maps for the six different GOC simulations of Table 1 would require six different 12 panel figures, the separation of the circulation induced by local and remote forcings is presented and discussed using the month of July as a representative example. Figure 3, which includes 12 months of the NGOC circulation, is shown and discussed in section 3.2.2.

[12] Figure 2 shows upper ocean PEBC from Cabo Corrientes (in the southeast corner) to the NGOC. These currents reach the maximum (secondary maximum) northward penetration into the NGOC during July (December–January) producing the primary (secondary) annual maximum in the northward transport [see *Zamudio et al.*, 2008, Figure 5]. The currents of Figure 2 are composed of (1) the CRCC that originates from a branch of the North Equatorial Counter Current that turns northward near the western coast of the Americas [*Wyrtki*, 1966; *Zamudio et al.*, 2001; *Kessler*, 2006], (2) the currents associated with the propagation of low-frequency CTWs [*Ripa*, 1997; *Strub and James*, 2002a, 2002b], and (3) the MCC that originates as the oceanic response to the local wind stress curl [*Zamudio et al.*, 2007; *Godínez et al.*, 2010]. Isolating the physical processes that contribute to the variability of the NGOC SSS is one of the main objectives of this study. Because the PEBC are proposed as the main transporters of low-salinity water from the Pacific to the NGOC, accuracy in the simulation of the PEBC is essential to simulate the GOC circulation, including the

NGOC seasonal reversal of the circulation, which was previously observed by *Lavín et al.* [1997] and modeled by *Beier and Ripa* [1999] and *Marinone* [2003] who used analytical wind and CTWs to force regional models. Here, we build upon these valuable model studies hypothesizing that the three components of the PEBC contribute to the generation of the NGOC seasonal reversing circulation. To test this hypothesis, the effects of the CRCC and the annual CTW on the generation of the NGOC seasonal reversing circulation are isolated by forcing the regional model with oceanic remote forcing only. Next, the effects of the MCC on the formation of the NGOC seasonal reversing circulation are isolated by forcing the regional model with local forcings only. Finally a third simulation is forced with both local and remote forcings. The different currents and CTWs included in these simulations are summarized in Table 1.

[13] There are several salient features of the simulations in Figure 2. All the simulations consist of upper ocean PEBC from Cabo Corrientes to the NGOC, a cyclonic circulation in the NGOC, and a series of eddies along the axis of the GOC. The two simulations forced with local plus remote forcing (Figures 2a and 2b) include the strongest and most continuous currents of all the simulations. This suggests positive coupling (strengthening) between the currents generated by local and remote forcings since the simulations forced with remote forcing only (Figures 2c and 2d) and local forcing only (Figures 2e and 2f) generate by themselves weaker summer GOC PEBC and weaker NGOC cyclonic circulation than the currents in Figures 2a and 2b. In addition to the PEBC, the simulations in Figures 2a–2d incorporate equatorward western boundary currents along the western coast of the GOC, from the NGOC to the southern tip of the Baja California Peninsula. These currents can mainly be attributed to the remote forcing because the equatorward western boundary currents are not evident in the simulations lacking remote forcing (Figures 2e and 2f). Furthermore, there are important differences in the magnitude of the currents modeled in the climatological and interannual simulations (Figure 2a versus Figure 2b, Figure 2c versus Figure 2d, and Figure 2e versus Figure 2f), which can be attributed to the effects of wind events and the interannual variability of the remote forcing. In short, both the local and the remote forcings act individually or together to induce upper ocean PEBC that penetrate into the NGOC and generate the observed summer cyclonic circulation.

3.2.2. NGOC Monthly Salinity and Circulation

[14] The monthly upper ocean currents of Figure 3 reveal a strong seasonal fluctuation in the circulation of the NGOC. That is distinguished by an overall seasonal reversal of the circulation. From November to April anticyclonic currents dominate the circulation in the NGOC. This anticyclonic circulation evolves from occupying the complete NGOC, including the circulation's center close to 113.6°W, 30.3°N and maximum current speed of ~15 cm/s during November (Figure 3k), to a more concentrated circulation with the center close to 113.8°W, 30°N and maximum current's speed of ~11 cm/s in April (Figure 3d). Furthermore, from November to April there is conclusive evidence of the effect of the PEBC on neither the anticyclonic circulation nor the SSS (Figure 4). That is an expected result, since the NGOC transport induced by the PEBC reaches the annual minimum during November [see *Zamudio et al.*, 2008, Figure 5] and consequently the
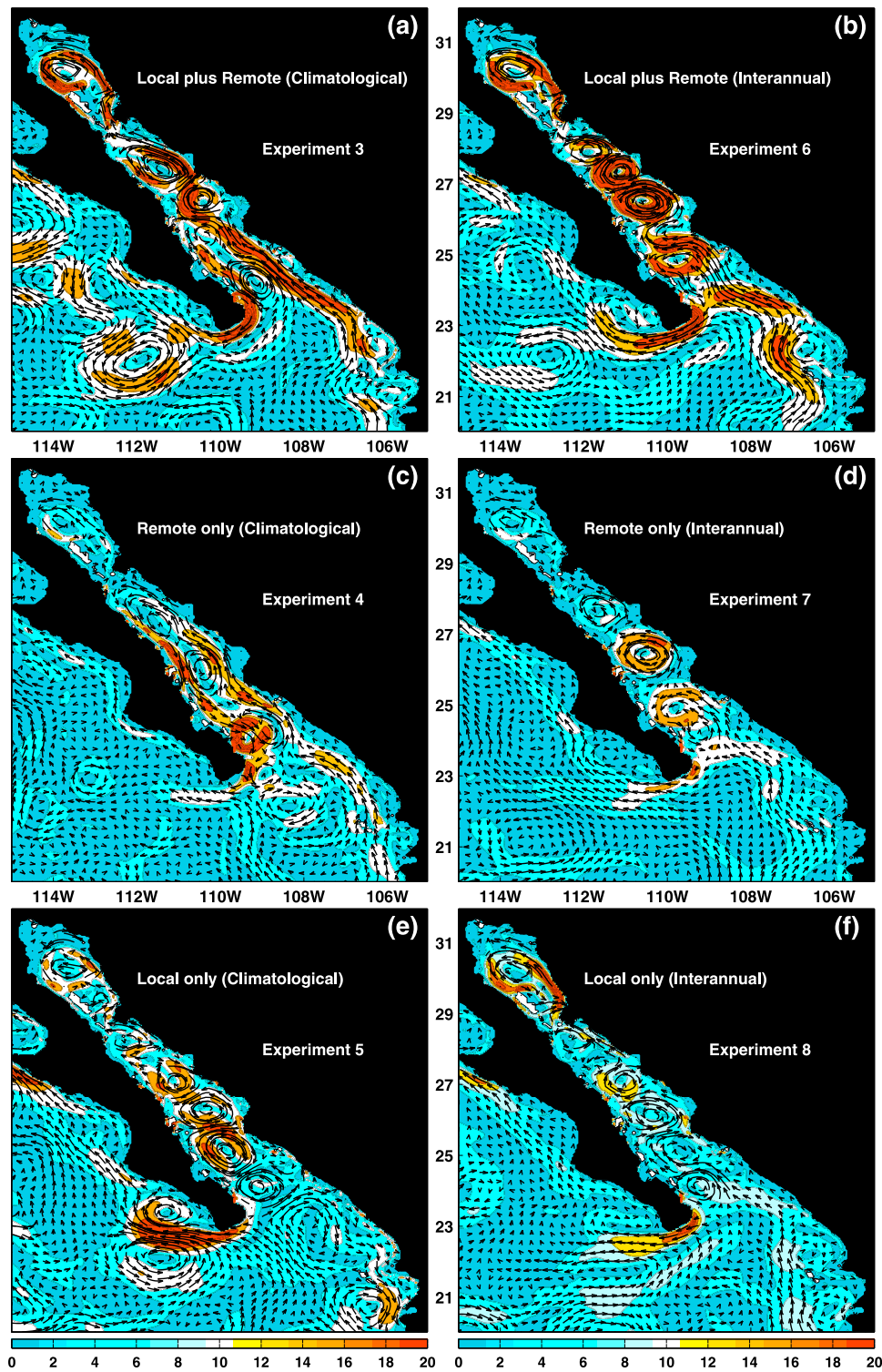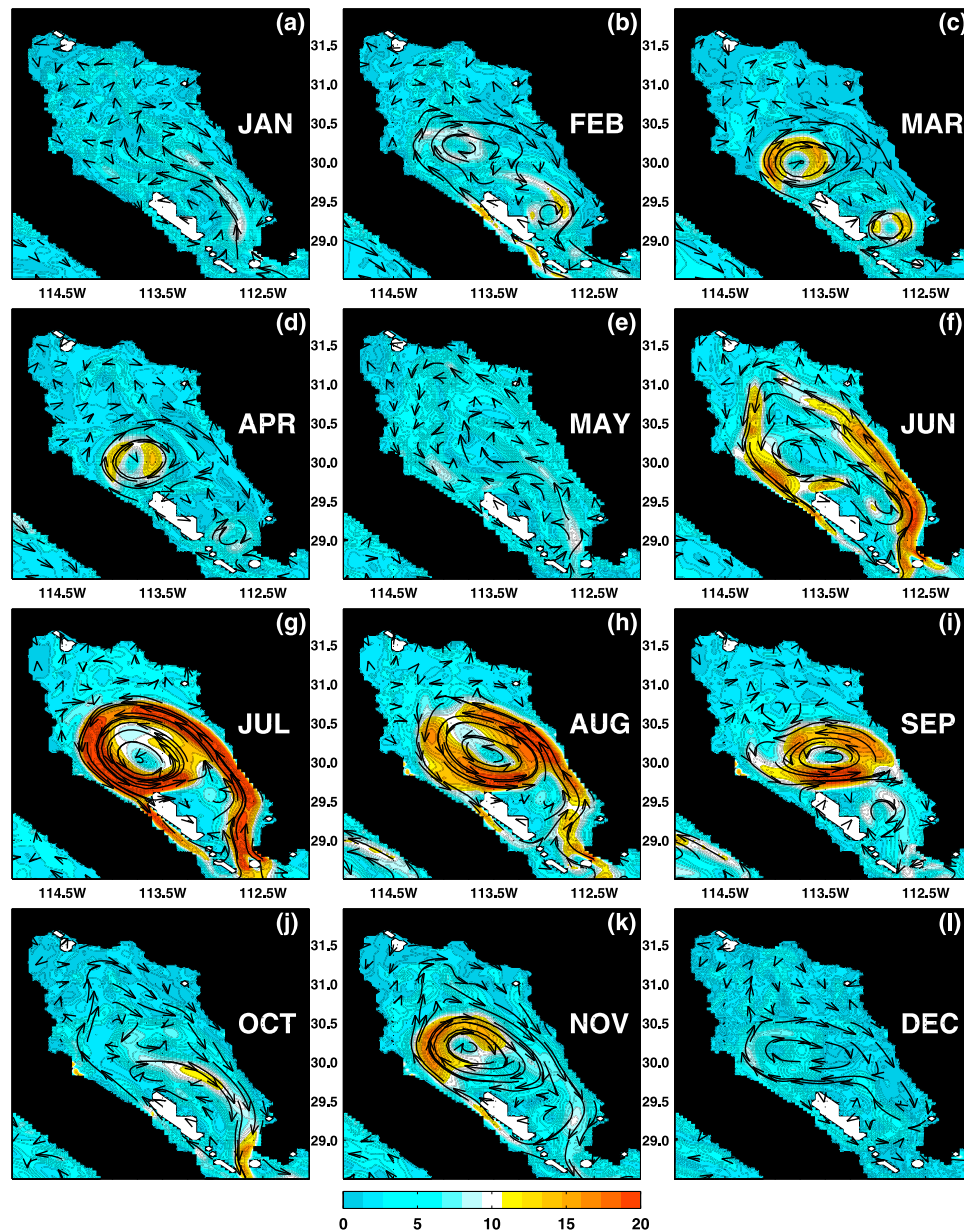
Figure 2. July mean upper ocean (0–100 m) currents as determined by six different nested GOC HYCOM simulations. The color contours (in cm/s) represent the magnitude of the currents and the arrow vectors represent the direction. The experiment number (described in Table 1) is indicated.

simulated SSS minimum is >35.8 from November to March (Figure 4). In addition, from November to March the NGOC is characterized by a general southeastward directed wind (Figure 4), which opposes the propagation of the PEBC weakening the northward penetration. Nevertheless, note the penetration of the PEBC to the NGOC during January that is consistent with the December–January secondary maximum of the northward transport [see *Zamudio et al.*, 2008, Figure 5]. In April the anticyclonic circulation starts to weaken due to the variation in the wind's direction that
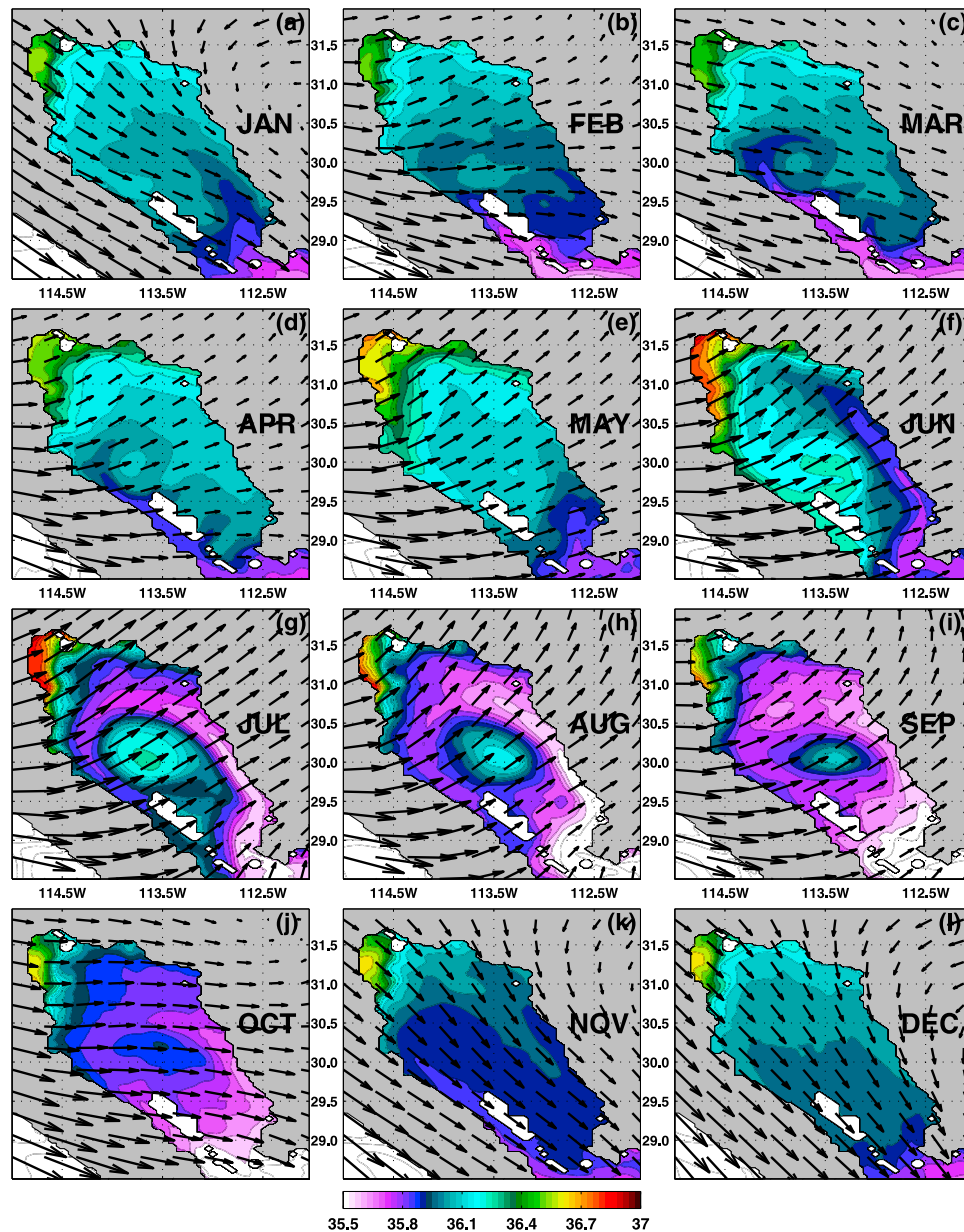
Figure 3. Monthly mean upper ocean (0–100 m) currents as determined by a climatologically forced nested GOC HYCOM simulation (experiment 3 in Table 1). The color contours (in cm/s) represent the magnitude of the currents and the arrow vectors represent the direction. White polygons are model land.

changes from southeastward directed to more eastward directed (Figures 3d and 4d). By May the PEBC starts to penetrate into the NGOC diminishing the anticyclonic circulation (Figure 3e). Thus, the transition month of May is characterized by a meandering poleward current. From June to September the wind blows in a general northeastward direction (Figures 4f–4i) and the NGOC features an upper ocean cyclonic circulation (Figures 3f–3i). During these summer months the upper ocean currents reach the maximum speed (~40 cm/s) for the year and the communication of the NGOC circulation with the southern GOC is more pronounced than during fall-winter, as evidenced by the low-SSS tongue extending cyclonically from along the coast from June to September (Figure 4f–4i). During the course of September the cyclonic circulation starts to weaken and by

the transition month of October the NGOC is characterized by a meandering equatorward circulation (Figure 3j).

[15] Overall, Figures 3 and 4 show that the influence of the Pacific Ocean and the southern GOC on the NGOC upper ocean circulation and SSS is stronger during spring-summer than during fall-winter. Furthermore, independent of the monthly SSS variability the maximum SSS is always located at the head of the upper NGOC and it reaches the yearly maximum during summer as measured by *Lavín et al.* [1998]. To provide some insight into the role of the PEBC as transporters of low-salinity water from the Pacific to the NGOC, we calculate the monthly maximum of the NGOC SSS for a simulation forced with local and remote forcings (thick line in Figure 5), and for a simulation forced with local forcings only (thin line in Figure 5). The two simulations capture the annual

Figure 4. Monthly mean sea surface salinity (color contours) as determined by a climatologically forced nested GOC HYCOM simulation (experiment 3 in Table 1) and 10 m wind stress (arrow vectors) simulated by NOGAPS. White polygons are model land.

cycle, but the simulation forced with local forcing only produces higher SSS than the simulation forced with local plus remote forcings. A plausible explanation for this result is as follows. The high evaporation in the NGOC generates high-SSS water and the PEBC modulates the generation of the high-SSS water by transporting upper ocean low-salinity water from the Pacific to the NGOC as shown in Figure 1c. The high evaporation and the MCC are included in the two simulations of Figure 5a. However, the CTWs and the CRCC (which transport low-salinity water from the coastal regions of Southern Mexico to the GOC (Animation 1[1] and section 3.3)) are only incorporated in the simulation with
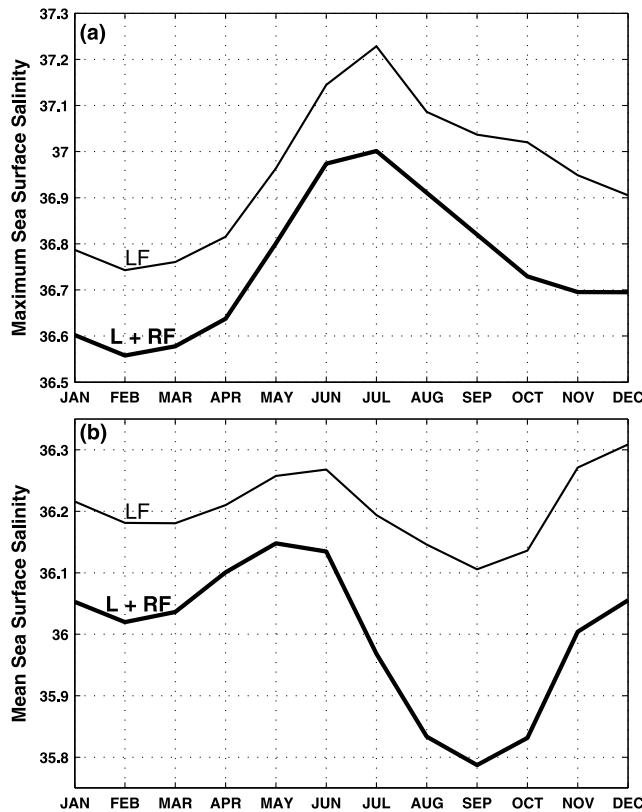
remote forcings (thick line in Figure 5a). Furthermore, it is important to recognize the dominance of the local forcing on the NGOC SSS monthly maximum regardless of the influence of the PEBC freshwater transport (Figure 5a). Equally significant are the effects of the PEBC freshwater transport on amplifying the semiannual cycle of the NGOC SSS monthly mean (Figure 5b).

3.3. Interannual Variability of the Salinity

[16] The NGOC HYCOM simulated SSS for the period 2003–2009 shows strong interannual variability (Figure 6a). As a response to the high evaporation in the NGOC (Figure 6b), water with salinities >36 is generated at the sea surface during the 7 years of this study (Figure 6a). Indeed, in

___
[1]Animation 1 is available in the HTML.

Figure 5. Time series of (a) monthly maximum and (b) monthly mean sea surface salinity for the NGOC region shown in Figure 4, as determined by a climatological simulation forced with local plus remote forcing (thick line labeled as L + RF is experiment 3 in Table 1) and by a climatological simulation forced with local forcing only (thin line labeled as LF is experiment 5 in Table 1).

2005 the maximum SSS reaches salinities >36.3, and during 2003 and 2007 it reaches salinities >36.2. In contrast, during 2006 and 2008 the minimum SSS reaches salinities <35.7 (Figure 6a). Why do 2005 and 2007 have the saltiest water of the period 2003–2009? Why are 2006 and 2008 characterized by the freshest water? Answers to these questions are presented and discussed in sections 3.3.1 and 3.3.2.

3.3.1. Evaporation as the Essential Generator and Modulator of the NGOC Salinity

[17] Assuming that the interannual variability in the generation of the NGOC high-salinity water is predominantly due to evaporation we would expect to see interannual variability in NGOC evaporation, which would have higher evaporation during 2003, 2005, and 2007 and lower evaporation during 2006 and 2008. To test this hypothesis we analyzed the interannual variability of the evaporation over the NGOC region (Figure 6b). Contrary to this hypothesis, 2006 exhibits the highest evaporation of the period 2003–2009. In addition, there is a lack of high-evaporation events concurrent with the high-salinity events of 2003, 2005, and 2007. These results suggest that evaporation is not always the dominant forcing on the generation of the upper ocean high-salinity water in this region as previously suggested by *Bray* [1988], *Lavín et al.* [1995], and *López* [1997]. Instead, another process modifying salinity must be driving these

events. In section 3.3.2, we show that lateral advection of salinity can explain these anomalies.

[18] Before moving to section 3.3.2, it is important to note that according to the Japanese Meteorological Agency El Niño-La Niña index [*Japanese Meteorological Agency*, 1991], an El Niño event was taking place in the Pacific Ocean during 2006. Concurrently, *Bray* [1988] reported an increase in the NGOC evaporation during El Niño years, which agrees with the high evaporation of 2006 of Figure 6b. Although the evaporation time series of Figure 6b is in agreement with *Bray*'s [1988] results, it does not explain the presence of the fresh water during 2006.

3.3.2. Evaporation and Volume Transport as the Generators and Modulators of the NGOC Salinity

[19] Time series of upper ocean transport along a zonal line across the entrance of the GOC is shown in Figure 6c. The 2006 El Niño event generated the second largest anomalous northward upper ocean transport over this period. This increase in the transport is consistent with the studies of *Strub and James* [2002a, 2002b] and *López et al.* [2005] who also reported an increase in the anomalous northward upper ocean transport into the GOC during the 1997 El Niño event. According to the Japanese Meteorological Agency index, 2003 and 2005 were classified as neutral years. However, those years include the strongest upper ocean southward transport events of the period 2003–2009. Why does the upper ocean northward transport into the GOC increase (decrease) during El Niño (La Niña) years?

[20] During El Niño (La Niña) years the equatorial Pacific features the formation of downwelling (upwelling) Kelvin waves. These waves propagate eastward until they reach the west coast of the Americas, where they excite poleward propagating coastal trapped waves with the northward CTWs reaching the GOC and beyond [*Spillane et al.*, 1987; *Enfield*, 1987; *Kessler et al.*, 1995; *Ramp et al.*, 1997; *Lyman and Johnson*, 2008]. The along coast SSH diagram of Figure 7 clearly shows these equatorial-originated waves propagating along the North Americas West Coast (from the Acapulco region to the NGOC). Downwelling (upwelling) CTWs induce poleward (equatorward) currents during their propagation in the GOC. Thus, the currents generated by these El Niño (La Niña) induced CTWs strengthen (weaken) the local PEBC and their associated upper ocean transport. That is displayed by the along coastal SSS anomaly diagram of Figure 8, which shows anomalously fresh surface water being advected poleward by the 2006 El Niño intensified CTWs. In concordance with this explanation, the hydrographic observations of *López et al.* [2005] and *Padilla et al.* [2006] clearly show upper ocean low-salinity water in the NGOC during the 1997 El Niño event [see *López et al.*, 2005, Figure 9]. Furthermore, it is important to note that although the amplitude of equatorially originated CTWs is generally increased during El Niño-La Niña years, these waves are also evident during neutral years (Figure 7). That is exemplified by the arrival of strong upwelling (downwelling) CTWs to the GOC during the 2003 (2008) neutral year (Figure 7), which forced anomalous upper ocean southward (northward) transport (Figure 6c), and the consequently maximum (minimum) in the SSS in the NGOC (Figures 6a and 8). In fact, the largest anomalous northward upper ocean transport over the period 2003–2009 occurred during the neutral year of 2008 and that
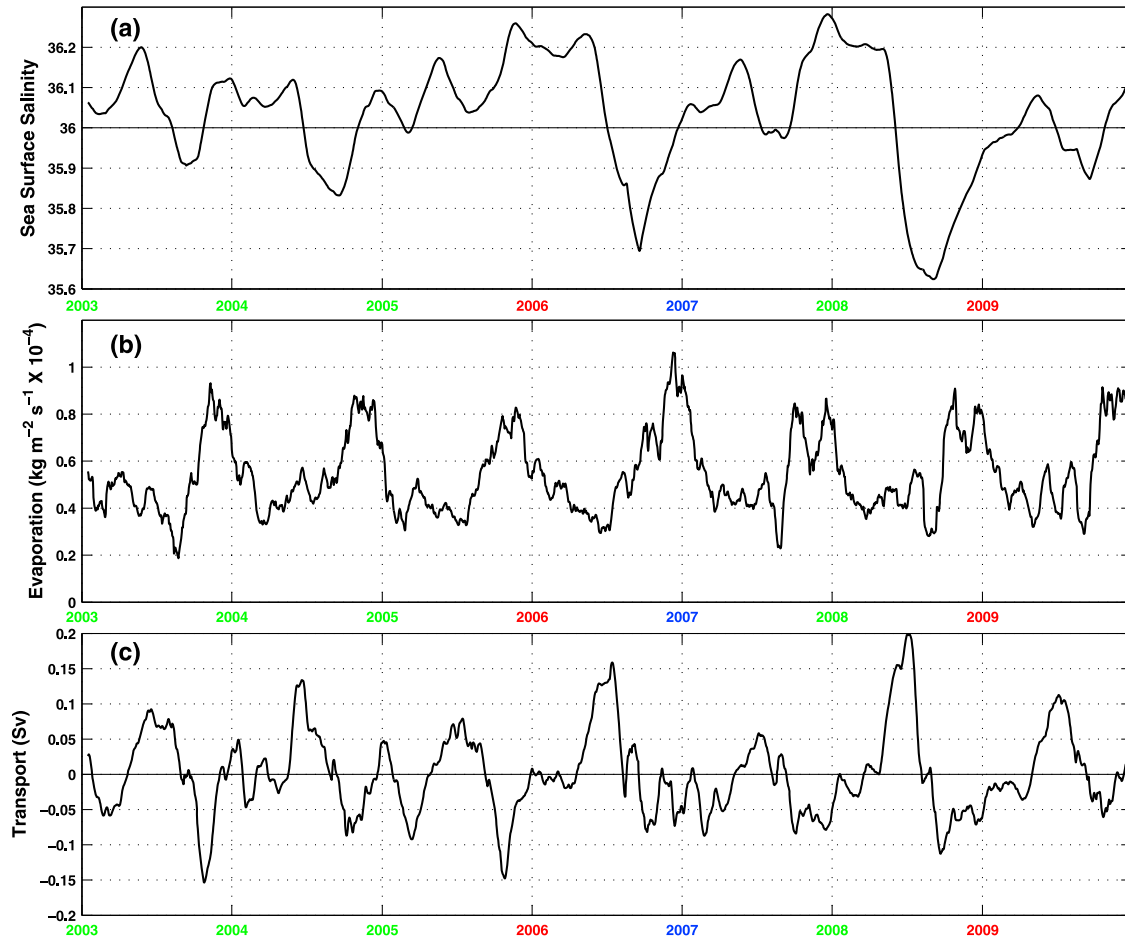
Figure 6. (a) Time series of daily mean sea surface salinity for the NGOC region shown in Figure 4. (b) Time series of daily mean evaporation for the NGOC region shown in Figure 4. (c) Time series of daily mean upper ocean (0–100 m) transport (Sv) calculated along the zonal line across the entrance of the GOC, which is indicated in Figure 1c. Positive transport indicates northward flow. The fields were determined by an interannually forced nested GOC HYCOM simulation (experiment 6 in Table 1). A 30 day running mean filter has been applied to the three time series. In accordance with the Japanese Meteorological Agency El Niño-La Niña index, El Niño, La Niña, and neutral years are represented with red, blue, and green colors, respectively. The first day of each year is labeled.
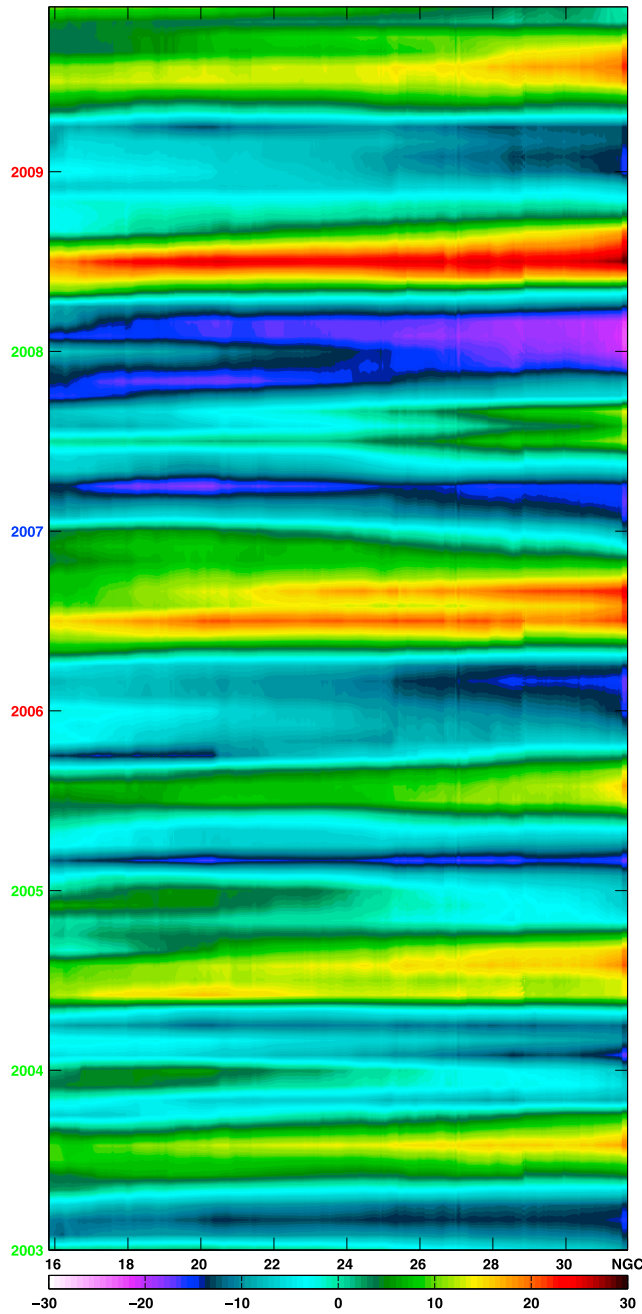
Figure 7. Sea surface height anomaly (color contours in cm) time series determined with an interannually forced nested GOC HYCOM simulation (experiment 6 in Table 1) along the west coast of Mexico, from 16°N to the northern Gulf of California. The anomaly is relative to the 2003–2009 mean. In accordance with the Japanese Meteorological Agency El Niño-La Niña index, El Niño, La Niña, and neutral years are represented with red, blue, and green colors, respectively. The first day of each year is labeled. NGC represents the location of the northern Gulf of California.
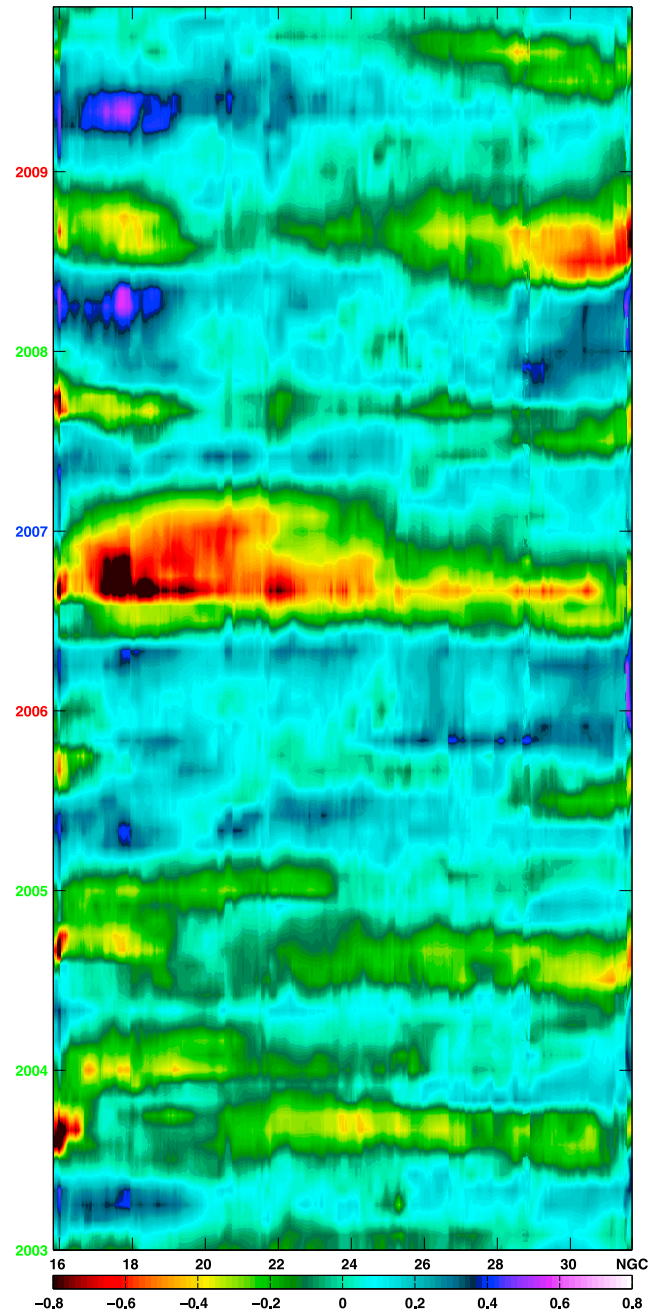
Figure 8. Sea surface salinity anomaly (color contours) time series computed from an interannually forced nested GOC HYCOM simulation (experiment 6 in Table 1) along the west coast of Mexico, from 16°N to the northern Gulf of California. The anomaly is relative to the 2003–2009 mean. In accordance with the Japanese Meteorological Agency El Niño-La Niña index, El Niño, La Niña, and neutral years are represented with red, blue, and green colors, respectively. The first day of each year is labeled. NGC represents the location of the northern Gulf of California.

transport event has a clear signature in the NGOC salinity (Figures 6a, 6c, and 8).

[21] Overall, the PEBC transport upper ocean low-salinity water from the Pacific to the GOC and that transport of low-salinity water is modulated by equatorially originated CTWs. Thus, the PEBC are the provider of low-salinity surface water. That water is used as the background conditions by the NGOC high evaporation to generate the NGOC high-salinity surface water.

4. Summary and Concluding Remarks

[22] The seasonal and interannual variability of the NGOC salinity is studied using an eddy-resolving (1/25° horizontal resolution) GOC version of HYCOM nested in global HYCOM. The nested approach (instead of a pure regional approach) permits the free communication of the NGOC with the Pacific Ocean. The NGOC salinity fluctuations are examined and they are controlled by both the NGOC high-evaporation and the low-salinity water transported by the PEBC from the Pacific to the NGOC. Model results indicate that the high evaporation generates high-salinity surface waters, which are featured by maxima SSS at the head of the upper NGOC and decreasing SSS toward the mouth of the GOC. The role of the three components of the PEBC (CRCC, MCC, and CTWs) on the NGOC seasonal circulation reversal is isolated. The model results suggest that besides the wind and the annual CTW as the main forcing of the seasonal reversal of the circulation [*Beier and Ripa*, 1999; *Marinone*, 2003] the CRCC and the MCC also contribute to the generation of the NGOC seasonal circulation reversal (Figure 2). Furthermore, the influence of the Pacific Ocean and the Southern GOC (via CRCC, MCC, and annual CTW) over the NGOC upper ocean circulation and SSS is stronger during spring-summer than during fall-winter (Figures 2–4).

[23] The NGOC SSS is characterized by strong interannually variability. Opposite to our initial hypothesis, the interannual variability of the NGOC SSS cannot be explained exclusively in terms of high evaporation. In fact, the second lowest SSS of the period 2003–2009 occurred during 2006, which was characterized by the highest evaporation of the period 2003–2009. That is reconciled by the second largest upper ocean northward transport of low-salinity water carried by the 2006 El Niño intensified PEBC (Figures 6–8). In short, on both seasonal and interannual time scales, high evaporation generates high salinity and the PEBC modulate the salinity by transporting upper ocean low-salinity water from the Pacific to the NGOC (Animation 1).

References

Alvarez-Borrego, S., and R. Schwartzlose (1979), Masas de agua del Golfo de California, *Cienc. Mar.*, 6, 43–63.

Argote, M. L., A. Amador, M. F. Lavı'n, and J. R. Hunter (1995), Tidal dissipation and stratification in the Gulf of California, *J. Geophys. Res.*, 100, 16,103–16,118, doi:10.1029/95JC01500.

Badan-Dangon, A., C. E. Dorman, M. A. Merrifield, and C. D. Winant (1991), The lower atmosphere over the Gulf of California, *J. Geophys. Res.*, 96, 16,877–16,896, doi:10.1029/91JC01433.

Barron, C. N., and L. F. Smedstad (2002), Global river inflow within the Navy Coastal Ocean Model, paper presented at Oceans 2002 MTS, Ints. of Electr. and Electr. Eng., Biloxi, Miss., 29–31 Oct.

Beier, E., and P. Ripa (1999), Seasonal gyres in the northern Gulf of California, *J. Phys. Oceanogr.*, 29, 305–311, doi:10.1175/1520-0485(1999) 029<0305:SGITNG>2.0.CO;2.

Berón-Vera, F. J., and P. Ripa (2002), Seasonal salinity balance in the Gulf of California, *J. Geophys. Res.*, 107(C8), 3100, doi:10.1029/2000JC000769.

Bleck, R. (2002), An oceanic general circulation model framed in hybrid isopycnic-cartesian coordinates, *Ocean Modell.*, 4, 55–88, doi:10.1016/S1463-5003(01)00012-9.

Bleck, R., and S. G. Benjamin (1993), Regional weather prediction with a model combining terrain-following and isentropic coordinates. Part 1: Model description, *Mon. Weather Rev.*, 121, 1770–1785, doi:10.1175/1520-0493(1993)121<1770:RWPWAM>2.0.CO;2.

Bray, N. A. (1988), Water mass formation in the Gulf of California, *J. Geophys. Res.*, 93, 9223–9240, doi:10.1029/JC093iC08p09223.

Carbajal, N., A. Souza, and R. Durazo (1997), A numerical study of the ex-ROFI of the Colorado River, *J. Mar. Syst.*, 12, 17–33, doi:10.1016/S0924-7963(96)00086-3.

Carnes, M. R. (2009), Description and evaluation of GDEM-V3.0, Rep. NRL/MR/7330–09–9165, Nav. Res. Lab., Stennis Space Center, Miss.

Castro, R., A. S. Mascareñas, R. Durazo, and C. A. Collins (2000), Seasonal variation of the salinity and temperature at the entrance of the Gulf of California, Mexico, *Cienc. Mar.*, 26, 561–583.

Enfield, D. B. (1987), The intraseasonal oscillation in eastern Pacific sea levels: How is it forced?, *J. Phys. Oceanogr.*, 17, 1860–1876, doi:10.1175/1520-0485(1987)017<1860:TIOIEP>2.0.CO;2.

Godínez, V. M., E. Beir, M. F. Lavín, and J. A. Kurczyn (2010), Circulation at the entrance of the Gulf of California from satellite altimeter and hydrographic observations, *J. Geophys. Res.*, 115, C04007, doi:10.1029/2009JC005705.

Japanese Meteorological Agency (1991), Climate charts of sea surface temperatures of the western North Pacific and the global ocean, technical report, 51 pp., Mar. Div., Tokyo.

Kallberg, P., A. Simmons, S. Uppala, and M. Fuentes (2004), The ERA-40 archive, *ERA-40 Proj. Rep. Ser. 17*, Eur. Cent. for Medium-Range Weather Forecasts, Reading, U. K.

Kara, A. B., H. E. Hurlburt, and A. J. Wallcraft (2005a), Stability-dependent exchange coefficients for air-sea fluxes, *J. Atmos. Oceanic Technol.*, 22, 1080–1094, doi:10.1175/JTECH1747.1.

Kara, A. B., A. J. Wallcraft, and H. E. Hurlburt (2005b), Sea surface temperature sensitivity to water turbidity from simulations of the turbid Black Sea using HYCOM, *J. Phys. Oceanogr.*, 35, 33–54, doi:10.1175/JPO-2656.1.

Kara, A. B., A. J. Wallcraft, P. J. Martin, and R. L. Pauley (2009), Optimizing surface winds using QuikSCAT measurements in the Mediterranean Sea during 2000–2006, *J. Mar. Syst.*, 78, S119–S131, doi:10.1016/j.jmarsys.2009.01.020.

Kessler, W. S. (2006), The circulation of the eastern tropical Pacific: A review, *Prog. Oceanogr.*, 69, 181–217, doi:10.1016/j.pocean.2006.03.009.

Kessler, W. S., M. J. McPhaden, and K. M. Weickmann (1995), Forcing of intraseasonal Kelvin waves in the equatorial Pacific, *J. Geophys. Res.*, 100, 10,613–10,631, doi:10.1029/95JC00382.

Lavín, M. F., and S. Organista (1988), Surface heat flux in the northern Gulf of California of California, *J. Geophys. Res.*, 93, 14,033–14,038, doi:10.1029/JC093iC11p14033.

Lavín, M. F., and S. Sánchez (1999), On how the Colorado River affected the hydrography of the upper Gulf of California, *Cont. Shelf Res.*, 19, 1545–1560, doi:10.1016/S0278-4343(99)00030-8.

Lavín, M. F., G. Gaxiola-Castro, J. M. Robles, and K. Richter (1995), Winter water masses and nutrients in the northern Gulf of California, *J. Geophys. Res.*, 100, 8587–8605, doi:10.1029/95JC00138.

Lavín, M. F., R. Durazo, E. Palacios, M. L. Argote, and L. Carrillo (1997), Lagrangian observations observations of the circulation in the northern Gulf of California, *J. Phys. Oceanogr.*, 27, 2298–2305, doi:10.1175/1520-0485(1997)027<2298:LOOTCI>2.0.CO;2.

Lavín, M. F., V. M. Godínez, and L. G. Alvarez (1998), Inverse-estuarine features of the upper Gulf of California, *Estuarine Coastal Shelf Sci.*, *47*, 769–795, doi:10.1006/ecss.1998.0387.

López, M. (1997), A numerical simulation of water mass formation in the northern Gulf of California during winter, *Cont. Shelf Res.*, *17*, 1581–1607, doi:10.1016/S0278-4343(97)00027-7.

López, M., L. Zamudio, and F. Padilla (2005), Effects of the 1997–1998 El Niño on the exchange of the northern Gulf of California, *J. Geophys. Res.*, *110*, C11005, doi:10.1029/2004JC002700.

Lyman, J. M., and G. C. Johnson (2008), Equatorial Kelvin wave influences may reach the Bering Sea during 2002 to 2005, *Geophys. Res. Lett.*, *35*, L14607, doi:10.1029/2008GL034761.

Marinone, S. G. (2003), A three-dimensional model of the mean and seasonal circulation of the Gulf of California, *J. Geophys. Res.*, *108*(C10), 3325, doi:10.1029/2002JC001720.

Metzger, E. J., H. E. Hurlburt, X. Xu, J. F. Shriver, A. L. Gordon, J. Sprintall, R. D. Susanto, and H. M. van Aken (2010), Simulated and observed circulation in the Indonesian Seas: 1/12° global HYCOM and INSTANT observations, *Dyn. Atmos. Oceans*, *50*, 275–300, doi:10.1016/j.dynatmoce.2010.04.002.

Padilla, F., M. López, J. Ochoa, and J. Sheinbaum (2006), Hydrographic and geostrophic currents in the northern Gulf of California during the 1997–1998 El Niño, *Cont. Shelf Res.*, *26*, 1154–1170, doi:10.1016/j.csr.2006.03.005.

Ramp, S. R., J. L. McClean, C. A. Collins, A. J. Semtner, and K. A. S. Hays (1997), Observations and modeling of the 1991–1992 El Niño signal off central California, *J. Geophys. Res.*, *102*, 5553–5582, doi:10.1029/96JC03050.

Reyes, A. C., and M. F. Lavín (1997), Effects of the autumn-winter meteorology upon the surface heat loss in the northern Gulf of California, *Atmósfera*, *10*, 101–123.

Ripa, P. (1997), Toward a physical explanation of the seasonal dynamics and thermodynamics of the Gulf of California, *J. Phys. Oceanogr.*, *27*, 597–614, doi:10.1175/1520-0485(1997)027<0597:TAPEOT>2.0.CO;2.

Rosmond, T. E., J. Teixeira, M. Peng, T. F. Hogan, and R. Pauley (2002), Navy Operational Global Atmospheric Predictions System (NOGAPS): Forcing for ocean models, *Oceanography*, *15*, 99–108.

Spillane, M. C., D. B. Enfield, and J. S. Allen (1987), Intraseasonal oscillations in sea level along the west coast of the Americas, *J. Phys. Oceanogr.*, *17*, 313–325, doi:10.1175/1520-0485(1987)017<0313:IOISLA>2.0.CO;2.

Steele, M., R. Morley, and W. Ermold (2001), PHC: A global ocean hydrography with a high quality Arctic Ocean, *J. Clim.*, *14*, 2079–2087, doi:10.1175/1520-0442(2001)014<2079:PAGOHW>2.0.CO;2.

Strub, P. T., and C. James (2002a), Altimeter-derived surface circulation in the large-scale NE Pacific gyres: Part 2. 1997–1998 El Niño anomalies, *Prog. Oceanogr.*, *53*, 185–214, doi:10.1016/S0079-6611(02)00030-7.

Strub, P. T., and C. James (2002b), The 1997–1998 oceanic El Niño signal along the southeast and northeast Pacific boundaries—An altimetric view, *Prog. Oceanogr.*, *54*, 439–458, doi:10.1016/S0079-6611(02)00063-0.

Wyrtki, K. (1966), Oceanography of the eastern equatorial Pacific Ocean, *Oceanogr. Mar. Biol. Annu. Rev.*, *4*, 33–68.

Zamudio, L., A. P. Leonardi, S. D. Meyers, and J. J. O'Brien (2001), ENSO and eddies on the southwest coast of Mexico, *Geophys. Res. Lett.*, *28*, 13–16, doi:10.1029/2000GL011814.

Zamudio, L., H. E. Hurlburt, E. J. Metzger, and C. Tilburg (2007), Tropical waves induce oceanic eddies at Cabo Corrientes and the María Islands Mexico, *J. Geophys. Res.*, *112*, C05048, doi:10.1029/2006JC004018.

Zamudio, L., P. J. Hogan, and E. J. Metzger (2008), Summer generation of the southern Gulf of California eddy train, *J. Geophys. Res.*, *113*, C06020, doi:10.1029/2007JC004467.

Zamudio, L., E. J. Metzger, and P. J. Hogan (2010), Gulf of California response to Hurricane Juliette, *Ocean Modell.*, *33*, 20–32, doi:10.1016/j.ocemod.2009.11.005.

P. Hogan and E. J. Metzger, Naval Research Laboratory, Code 7323, Stennis Space Center, MS 39529, USA.

L. Zamudio, Center for Ocean-Atmospheric Prediction Studies, Florida State University, Tallahassee, FL 32306-2840, USA. (luis.zamudio.ctr.mx@nrlssc.navy.mil)